JJMIE

Volume 4, Number 6, December 2010
ISSN 1995-6665
Pages 665- 676

Jordan Journal of Mechanical and Industrial Engineering www.jjmie.hu.edu.jo

Numerical Modelling of a Turbocharger Splitter-Vaned Centrifugal Impeller at off-Design Conditions Part II: Computation of Forces and Torques

A. Fatsis [a], A. Panoutsopoulou [b], N.Vlachakis [a]

[(a)] *Technological University of Chalkis, Department of Mechanical Engineering, 34400 Psachna, Evoias, Greece.*

[(b)] *Hellenic National Defence Systems S.A., 1, Ilioupoleos Avenue, 17236, Greece*

Abstract

Forces and torques acting on each individual blade and on the shaft of a centrifugal impeller with splitter vanes working at off-design conditions, are computed by using the pressure integration and the momentum balance method. Two cases are examined simulating the operation of a centrifugal compressor at higher mass flows than the optimum one: the first where the Strouhal number, $S_r = 0.146$, corresponds to subsonic flow inside the impeller and the second one where the Strouhal number, $S_r = 0.225$, corresponds to transonic flow inside the impeller. For the first case, the variation of forces is more distinct in the circumferential location where the volute tongue is located. For the second case a bimodal distribution is observed per impeller rotation. Calculations done for impellers with backward leaned blades and with radial ending blades demonstrate the influence of the impeller exit geometry to the radial force.

Keywords: radial force, unsteady forces, centrifugal impeller, splitter blades.

Nomenclature

c	Speed of sound
f	Frequency
t	Time
$\vec{F}$	Force
L	Length of blade channel
M	Mach number
P	Static pressure
$\vec{S}$	Surface
S_r	Strouhal number
T	Torque
$\vec{V}$	Absolute velocity
ρ	Density

Superscripts

bl	Blade
spl	Splitter
01	Total conditions at the impeller inlet

Subscripts

m	Meridian
ps	Blade or splitter pressure side
r	Radial
rel	Relative
ss	Blade or splitter suction side
st	Static
z	Axial
θ	Circumferential
1	Impeller inlet
2	Impeller trailing edge

1. Introduction

When centrifugal compressors work at off-design conditions, the volute type collector creates a circumferentially non-uniform static pressure distribution at the diffuser exit. In case of a vaneless diffuser, the pressure distortion propagates upstream and creates unsteady flow inside the impeller, [1]. This results to a

circumferential variation of the blade loading and fluctuating forces acting on the impeller blades. A first consequence is a non-zero radial force on the impeller shaft and extra load on the bearings. It also means unsteady flow and forces in the rotating blade passages resulting in blade vibrations and additional noise. This increases losses and decreases the operating range of the compressor.

Initially researchers experienced the existence of radial forces exerted on the shaft of centrifugal pumps when they operated at mass flows different from the design one because of failure of the bearings supporting the impeller shaft, [2]. Experimental determination of the magnitude and direction of radial forces acting on the bearings supporting the impeller shaft was done by measuring the bearing reaction [3]. At lower specific speeds there is a relatively large flow rate range over which the minimum force is essentially constant. For higher specific speeds the radial force has a minimum almost at a single point. Deviating on both sides of that point, the rate of increase of the radial force is high. This means that for high specific speeds, a small deviation from the design point is sufficient to create large radial forces, and accordingly a large radial thrust on the bearings of the impeller shaft. The point corresponding to the minimum radial force does not necessarily correspond to 100% design flow rate because the design of the volute may produce circumferentially uniform static pressure at higher or lower mass flow rates, [3].

The effect of the number of blades on the magnitude of the radial force was studied experimentally, [4]. It was found that the magnitude of the radial thrust of the seven-bladed impeller is larger than the one of the three-bladed impeller. On the contrary, the fluctuating range doubles in the case of the three-bladed impeller compared to the seven-bladed impeller.

Empirical investigations were also attempted to correlate the magnitude of the radial force with geometrical data and volume flow rates or the specific speed for pumps [5,6,7]. All these empirical methods, assuming incompressible flows, even though present satisfactory results for the series of pumps that were applied, fail to provide a universal equation for all types of centrifugal pumps or compressors.

A simple numerical model to compute the radial force caused by a volute casing acting on a pump impeller at design and off-design conditions was presented [8]. It was concluded that the magnitude of the predicted force increases linearly on either side of optimum mass flow. Larger discrepancies are observed at higher mass flows and at design point, than at lower mass flows. A simple 1D unsteady model was presented, able to predict the impeller response and radial force due to the circumferential static pressure variation caused by the volute, [9]. The model is applicable for incompressible flows and assumes a circumferentially constant relative outlet flow angle. This is in contrast to experimental observations, where circumferential variations in the relative outlet flow angle were measured.

Calculations of forces acting on blades and on the impeller shaft bearing were also done assuming 2D potential flow inside the impeller. The forces on blades were found by integrating the pressure field on the solid surfaces of the impeller [10]. There is no analysis of the different contributions to the radial force, because the pressure integration method they used can only give the total force and not its components. The prediction of the magnitude and direction of the forces shows a complete discrepancy with experimental results, [6]. This fact underlines the need of a fully unsteady model to investigate numerically the impeller response.

Two-dimensional unsteady flow numerical models are also found in the literature, aiming to study the centrifugal impeller response due to outlet static pressure distortion, by solving the 2D incompressible Navier Stokes equations and the 2D Euler equations respectively [11,12]. In both studies no information is given on the radial force magnitude and direction, neither on the contributions to this force. One of the limitations of 2D methods is that the three dimensional effects, which are present in the real flow inside a centrifugal impeller, are ignored.

A 3D numerical method was developed in order to study the unsteady flow field inside the impeller due to a circumferential variation of the static pressure at the impeller outlet, for the case of full-bladed impellers, [13]. The present study is an original contribution and the second part and an extension of the article of the same authors entitled ‘‘Numerical modelling of a turbocharger splitter-vaned centrifugal impeller at off-design conditions. Part I: Impeller flow field’’. The present article describes a method to predict forces acting on impeller blades, as well as radial force on the impeller shaft. Computations are performed for centrifugal impeller with splitter vanes, having backward leaned blades for lower and higher mass flows. The contributions to the forces are analysed and commented for impellers for backward leaned blades and for impellers with radial ending blades. Results obtained show that the predicted direction of the radial force is in agreement to experimental observations.

2. Unsteady Flow Computations

2.1. Unsteady flow model

The numerical model applied is well documented in [1,13] and only a summary of it will be given here.

The numerical model used to analyse the unsteady impeller flow field consists of the 3D Euler equations. Adopting the Euler equations means that the viscous terms from the full Navier-Stokes equations are neglected, and the transport of momentum and energy in the fluid is done only by means of convective fluxes. This means that viscous areas of the flow such as boundary layers developed along solid wall boundaries or wakes downstream the blades cannot be evaluated accurately by means of the present method. Since viscous forces are neglected, this implies that the considered model is not valid at relatively low rotational speed. Using the Euler equations compressible rotational flow, steady or unsteady flow fields can be calculated. This simplification results in an affordable computer time and gives useful information on the dynamics of the flow in the case where the impeller is not heavily loaded and flow separation is limited. The model was validated for the case of full-bladed centrifugal impeller, showing fairly good agreement against available

experimental results in the literature and predicting the unsteady flow features that are in agreement with experimental investigations, [1].

The 3D Euler equations in non-dimensional form are written in conservative form in cylindrical coordinates, *(r,θ,z)* as follows:

$$\frac{\partial \vec{u}}{\partial t}+\frac{1}{r}\cdot\frac{\partial\left(r\,f(\vec{u})\right)}{\partial r}+\frac{1}{r}\cdot\frac{\partial g(\vec{u})}{\partial \theta}+\frac{\partial h(\vec{u})}{\partial z}+\vec{b}(u)=0 \quad (1)$$

where $\vec{u}$ is the vector of conservative variables, $f(\vec{u}), g(\vec{u}), h(\vec{u})$ are the vectors of convective fluxes and $b(\vec{u})$ is the source term, defined in detail in [1]. The conservative formulation of the equations allows the accurate treatment of flow discontinuities such as shock waves in the flow field.

The space discretization of the equations, centred in space, is done by means of the finite volume technique, offering second order spatial accuracy in smooth grids, [1].

The partial differential equations are written in a semi-discrete form as follows:

$$\frac{d}{d\,t}\left(\vec{u}\right)+\vec{R}=0 \quad (2)$$

where $\vec{R}$ are the residuals of the equations. The Runge-Kutta four steps scheme, providing second order accuracy for non-linear partial differential equations and extensive stability limits up to a CFL number of $2\cdot\sqrt{2}$, was used for the time integration, offering a second order accuracy for non-linear problems. Extensive testing of the method in special test cases for which analytical solutions exist, has demonstrated the accuracy of this scheme for unsteady flow predictions, [2]. The time step used for the unsteady flow calculations is a constant one; it relates the rotational speed of the impeller to the number of grid points in the circumferential direction and it satisfies the stability limits of the CFL condition.

Impermeable wall boundary conditions are imposed on the solid walls (i.e. on the blade and splitter suction and pressure side and on the hub and shroud walls) by considering only the static pressure when computing the convective fluxes. At the inflow and outflow boundaries, non-reflecting boundary conditions based on the Fourier decomposition, were used, [13]. Non-reflecting boundary conditions suggest infinitely long pipes upstream and downstream of the impeller and it is shown in [13] that the solution is not affected by the upstream location of the inflow boundary. Since the outflow static pressure is not uniform along the circumference, this means that as the impeller rotates, a virtual point attached at the trailing edge experiences different values of the static pressure throughout a full rotation, which consists the period of the phenomenon. Phase-lagged periodicity conditions were used to simulate this non-uniformity and to compute the fluxes through the upstream and downstream streamlines. Figure 1 shows a meridional *(r-z)* projection, a blade-to-blade *(θ-z)* projection and a 3D view of the H-grid used for the calculations. The points in axial, radial and circumferential position were uniformly distributed and the splitter vane was put between two full blades. The consistency and stability analysis of the method are given in detail in [13] where the numerical scheme was presented in detail.

The model was validated for the cases of full-bladed and splitter-vaned centrifugal impeller, showing fairly good agreement against available experimental results in the literature and predicting the unsteady flow features which are in agreement with experimental investigations [1].

The blade-to-blade projection of the computational domain is shown in Figure 2. Continuous lines indicate the pressure side of a full blade and the suction side of a splitter vane and dashed lines the pressure side of the splitter vane and the suction side of the full blade. Phase-lagged periodicity conditions are used to update the upstream and downstream stagnation pseudo-streamlines AB, CD and EF, GH, respectively, [14]. Implementing phase-lagged periodicity conditions, data obtained from the same rotation, as well as data stored in the computer memory from the previous rotation have to be used. This slows down the convergence to a periodic solution. The points along the pseudo-streamlines upstream and downstream of the splitter vanes (namely KL, MN in Figure 2) are treaded as interior points of the numerical domain and simple continuity of the fluxes is imposed. From the same figure it can be observed that the upstream and downstream extension of the computational domain is reduced. This is due to the non-reflecting boundary conditions that used for the inflow and outflow boundaries, [1].

The acoustic Strouhal number can characterize unsteady compressible flows. It is defined as the product of the reduced frequency and the Mach number:

$$S_r = \frac{f\cdot L}{c} \quad (3)$$

where L is the length of a blade passage, whereas f is the number of rotations per second times the number of perturbation waves around the circumference and c is the speed of sound.

It relates the time needed by a pressure wave to travel a distance L, at the speed of sound c to the period of the pressure perturbation $1/f$. Unsteady effects are small for $Sr < 0.1$ and the flow can be evaluated by means of steady calculations. For $Sr > 0.1$ accurate results can be obtained only by means of unsteady flow calculations.

2.2. Convergence of the time accurate calculations

Computations of the unsteady flow field have as initial value the converged solution of the steady state case, where the static pressure at the impeller outflow is circumferentially uniform. Figure 3 shows the converged history of the time-dependent calculations. In such flows convergence is achieved when the circumferential distribution of a flow variable repeats itself after a rotation of the impeller.

From this figure it can be also observed that the imposed static pressure circumferential distribution (which repeats itself over a rotation of the impeller) has a saw tooth profile. This is a typical static pressure distribution for the case of higher mass flows and it is in agreement with experimental results [12]. Such a profile can be also obtained by using a 1D flow model, [9].

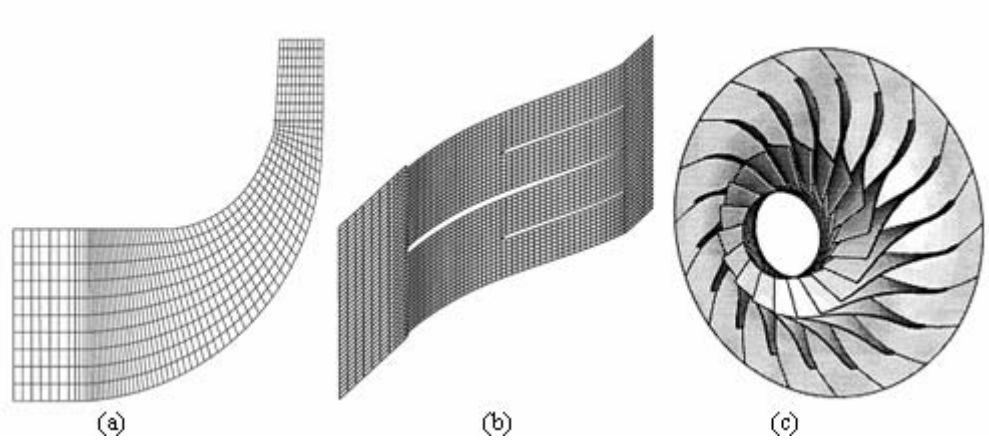

Figure 1: (a)Meridional *(r-z),* (b)Blade-to-blade *(θ-z)* view of the H-grid used for the calculations, (c)Three-dimensional view of the impeller blades

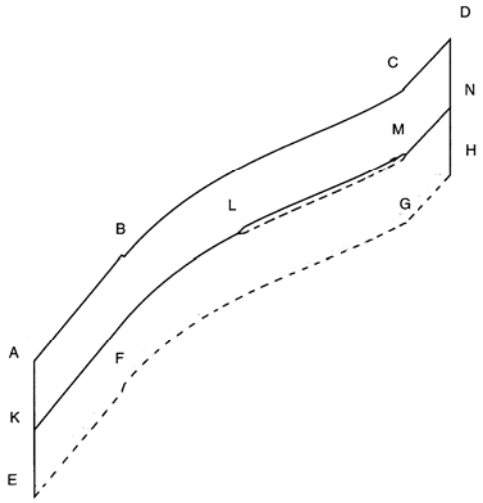

Figure 2: Blade-to blade *(θ-z)* projection of the computational domain used for the splitter-vaned impeller computations

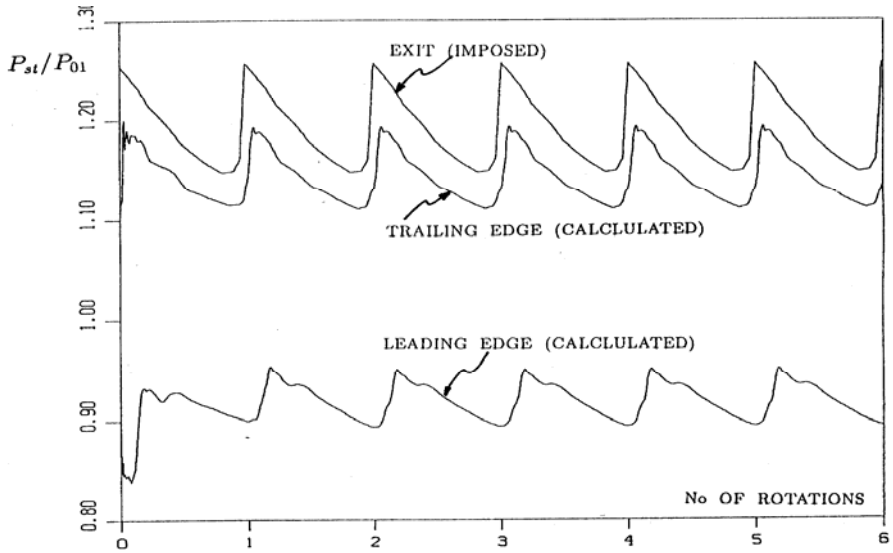

Figure 3: Convergence history of the unsteady flow calculations.

The calculated static pressure distribution at the leading edge shows decreased amplitude with respect to the imposed distribution. This is due to the time needed for a perturbation to propagate from the outlet to the inlet and is a consequence of the way the phase-lagged periodicity conditions are implemented. Information obtained at previous rotation is used when calculating the flow at the current one. Consequently, the results of the first rotation are partly influenced by the steady state solution and it takes several rotations before the unsteady flow is fully established everywhere. The static pressure profiles at trailing and leading edge are distorted by the pressure wave reflections in the impeller.

Figure 4 shows relative Mach number iso-lines in a blade-to blade development of the hub, mean and shroud surfaces of the impeller for transonic flow inside the impeller and $S_r = 0.225$. This figure comes by monitoring the blade channel of Figure 2 during one complete rotation of the impeller. Since the flow field is unsteady, monitoring the blade channel of Figure 2 during one rotation, one will observe different flow patterns and if only one full rotation is completed, he will find back the initial flow conditions. The Mach number variations at the shroud streamsuface are more pronounced than the ones at the hub streamsurface. Waves due to the exit static pressure distortion have to travel a longer path at hub than a shroud. In the later streamsurface the transonic region close to the leading edge suction side of the blade heavily influences them. The upstream-propagated static pressure distortion cannot pass through the transonic flow regime close to shroud suction surface and reflects downstream as a compression wave interacting with incoming pressure waves. The variations in Mach number indicate variations in static pressure and in blade loading during one period of the phenomenon. One can also see that the inflow and outflow boundaries are located close to the impeller.

This was made possible by using non-reflecting boundary conditions at the inlet and outlet boundaries [1].

3. Computation of Forces

3.1. General Formulations

A Cartesian coordinate system is used to define the forces and torques acting on each individual blade and on the impeller shaft. The *x*-axis is from the shaft centre towards the volute tongue, and the *y*-axis perpendicular to it. (Figure 5).

Two methods have been used to compute the forces and torques resulting from the outlet circumferential static pressure distortion.

The first one integrates the pressure over the whole impeller surface.

$$\vec{F} = \int\int P_{i,j,k}\, d\vec{S}_{i,j,k} \tag{4}$$

The total force is computed by adding the contribution of each blade separately. In case of an unshrouded impeller, the pressure on the shroud does not contribute to the forces on the shaft. In case of a shrouded impeller the pressure on the outer side of the shroud should also be integrated.

The second one is the momentum balance method. This method computes the total force acting on the impeller, and not on a single blade because the momentum balance gives the forces acting on the whole channel and not on each surface. The total force $\vec{F}$ is given by:

$$\vec{F}_{\Delta MR} + \vec{F}_{\Delta M\Theta} + \vec{F}_P = \vec{F} \tag{5}$$

where $\vec{F}_P$ is the force due to the static pressure at inlet and outlet section, $\vec{F}_{\Delta MR}$ and $\vec{F}_{\Delta M\Theta}$ are the forces due to the change of radial and tangential momentum. Written in summation form, the previous equation is:

$$\left(\sum_k\sum_j \rho_{i,j,k}\,\vec{V}_{i,j,k}\,\vec{S}_{i,j,k}\,\vec{V}_R\right)_{out} - \left(\sum_k\sum_j \rho_{i,j,k}\,\vec{V}_{i,j,k}\,\vec{S}_{i,j,k}\,\vec{V}_R\right)_{in} +$$
$$\left(\sum_k\sum_j \rho_{i,j,k}\,\vec{V}_{i,j,k}\,\vec{S}_{i,j,k}\,\vec{V}_\Theta\right)_{out} - \left(\sum_k\sum_j \rho_{i,j,k}\,\vec{V}_{i,j,k}\,\vec{S}_{i,j,k}\,\vec{V}_\Theta\right)_{in} + \tag{6}$$
$$\left(\sum_k\sum_j P_{i,j,k}\,\vec{S}_{i,j,k}\right)_{out} - \left(\sum_k\sum_j P_{i,j,k}\,\vec{S}_{i,j,k}\right)_{in} = \vec{F}$$

The indices *j, k* run from suction to pressure side and from hub to shroud, respectively. The flow velocity and static pressure at each circumferential position are the ones obtained from the computation of the unsteady flow field at a given impeller position.

Both methods predict different forces when applied to the same geometry using the results obtained with a coarse grid consisting of *43*11*11* points. Repeating both calculations on a finer grid having *86*15*15* points shows almost identical results, which are close to the ones obtained from the pressure integration method on a coarse grid, Figure 6. Similar results, but non shown in this paper, are obtained from the calculation of the Torque around the axis of the impeller, the torque around the *y*-axis and the axial force acting on the impeller. One can conclude from this that the momentum balance method is more sensitive to the grid density than the pressure integration method.

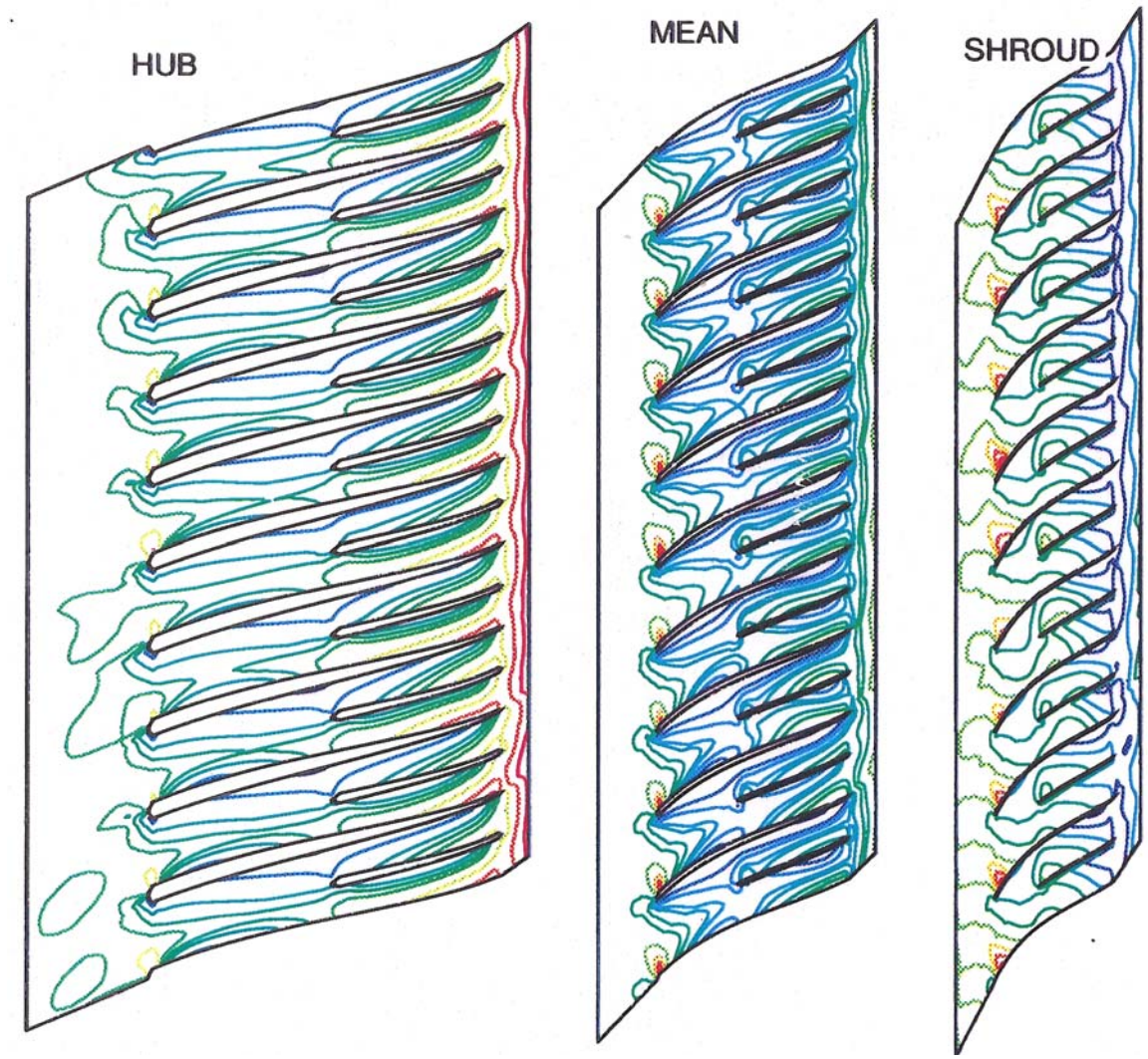

Figure 4: Iso-Mach lines for the hub, mean and shroud streamsurfaces of the impeller.

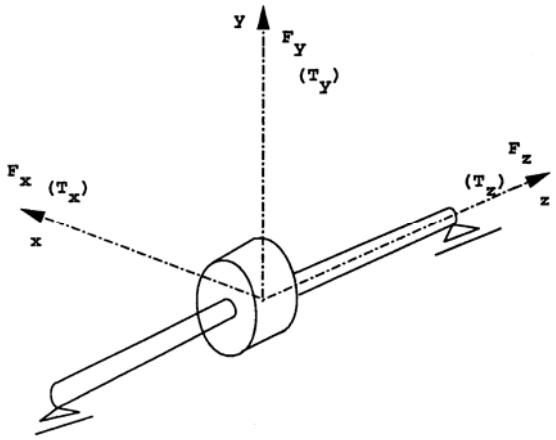

Figure 5: System of coordinates used to calculate forces and torques

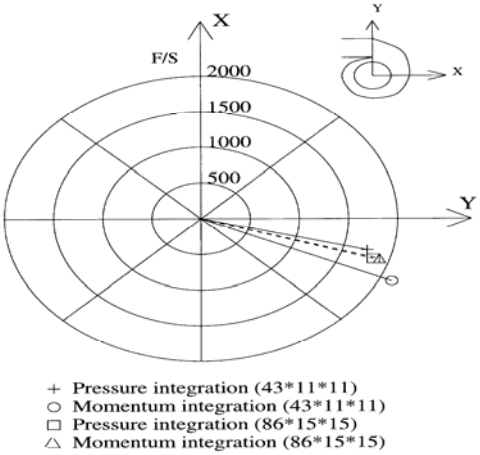

Figure 6: Radial force computation using the pressure integration method and the momentum integration method for two different types of grid density.

Although the momentum balance method does not allow the calculation of forces on individual blades, it allows the evaluation of the individual contributions to the radial force. This is important in the context of an experimental definition of the radial forces in function of the flow quantities at the impeller inlet and outlet. It can answer the question whether it is sufficient to integrate the static pressure distortion over the impeller outlet circumference or if one should also account for the variation in radial and tangential velocity.

3.2. Forces calculations at higher mass flows and different Strouhal numbers

3.2.1. Strouhal number 0.146 corresponding to subsonic flow inside the impeller.

Here, the circumferential variations of the axial, radial force acting on a single blade, and the torque around the z-axis of the impeller will be presented. These distributions are obtained by monitoring one blade during one impeller rotation.

The circumferential variations of the axial force, radial force acting on a single blade and the torque around the *z*-axis resulting from a single blade are shown in Figure 7. From this figure, one can see that there is a significant variation of the above forces and torques close to the tongue region (which corresponds to 33^o) due to the peak in the circumferential variation of static pressure. In regions of smooth variation of the static pressure, theses quantities vary smoothly as well.

3.2.2. Strouhal number 0.225 corresponding to transonic flow inside the impeller

The axial force, radial force acting on a single blade and the torque around z-axis resulting from a single blade are shown in Figure 8. From these figures, one can see that there is a bimodal variation of the above forces and torque as a result of the pressure waves reflected at the leading edge, travelling twice upstream and downstream the impeller during one rotation. This was also observed for the case of full-bladed centrifugal impeller operating at higher than optimum mass flows and a similar value of the acoustic Strouhal number, [1]. The two waves per rotation were even more clearly visible because the waves were not perturbed by reflections at the leading edge of the splitter vanes. The amplitude of the variation for the axial force, radial force and torque is larger than for the case of $S_r = 0.146$ discussed previously.

3.3. Calculations at higher and lower mass flows

In Figure 9 one can see the direction and magnitude of the individual components of the radial force in the case of higher (continuous lines) and lower (dashed lines) than design mass flow. The radial force vectors are for both cases in agreement with the experimental results, [16]. For both mass flows, the largest contribution to the radial force is the one resulting from the outlet static pressure. The force component due to non-uniform outlet radial momentum is much smaller and in the opposite direction, as it was concluded from the experimental data in [17].

It results in a decrease of the radial force. The inlet flow distortion also results in a non negligible contribution to the radial force.

3.4. Influence of the impeller geometry

The influence of the impeller geometry on the radial force is illustrated by comparing previous results with those on an impeller with radial ending blades, [1].

The difference in contribution to the radial force can be explained by means of Figure 10. The increase or decrease of the relative velocity is due to the disequilibrium between the pressure rise by the impeller and the imposed outlet pressure. In case of a backward leaned impeller any increase in relative velocity, because of a decrease in outlet pressure, provokes a decrease of tangential velocity and as a consequence a decrease in pressure. As a result, the disequilibrium between the imposed and impeller outlet static pressure gets smaller. This corrective action results in a smaller change in radial velocity and the circumferential variation of the radial momentum, which is proportional to V_{R2}^2, and its contribution to the radial force is smaller.

The pressure rise in radial ending impellers is less dependent of the radial velocity because it does not involve a variation in $V_{\Theta 2}$, so that the change in radial velocity and radial momentum, for a given pressure change, is much larger.

The different contributions of the tangential momentum at the impeller outlet can also be explained. The increase in radial velocity, due to a local decrease in static pressure, results in a decrease of the tangential velocity for backward leaned blades as indicated on Figure 10a. As a consequence, the product $\rho \cdot V_{m2} \cdot S \cdot V_{\Theta 2}$ is almost constant along the periphery. The contribution of the tangential momentum to the radial force is thus negligible for backward leaned impellers.

In case of radial ending blades, an increase in mass flow does not alter the tangential component of the absolute velocity $V_{\Theta 2}$ (dotted line velocity triangle in Figure 10b). The product $\rho \cdot V_{m2} \cdot S \cdot V_{\Theta 2}$ is not constant along the periphery because only V_{m2} changes. The outlet tangential momentum is therefore not uniform circumferentially, resulting in a significant contribution to the force. Its direction is almost perpendicular to the radial momentum force.

4. Conclusions

In the present study the numerical prediction of forces and torques on individual centrifugal splitter-vaned impeller blades was presented. The total force acting on the impeller is obtained by adding the forces on all blades and the hub surface.

In the case of a shrouded impeller the pressure on the inner and outer side of the shroud should also be integrated. The latter is not predicted by the Euler solver but can be obtained by a suitable model, e.g. [15].

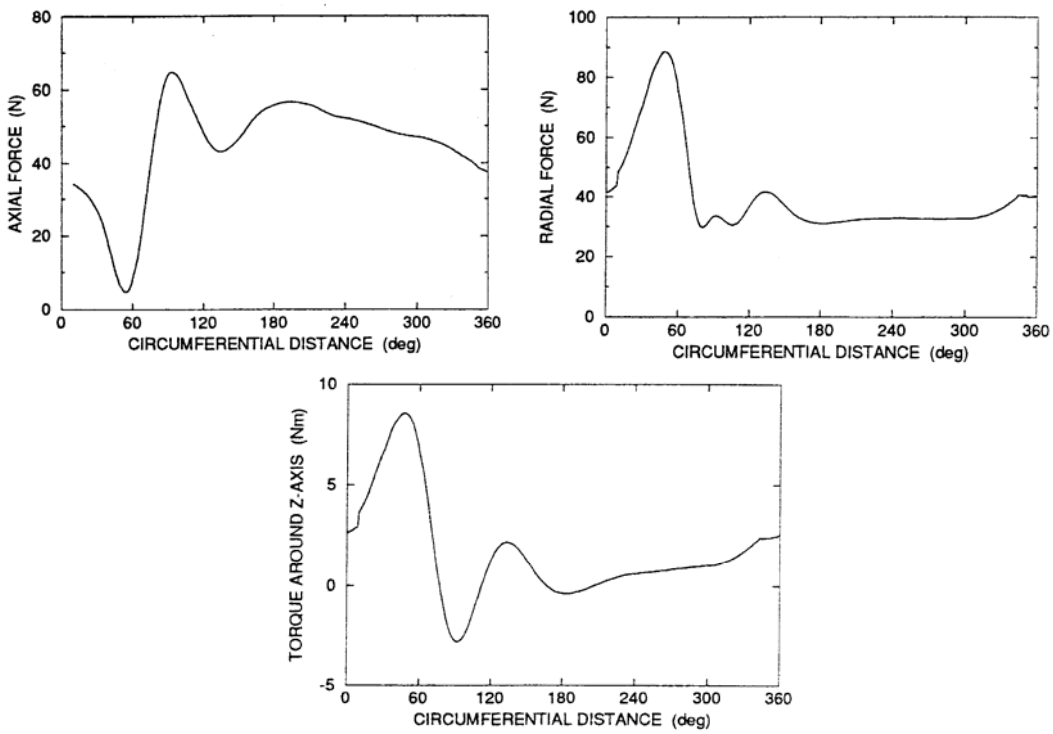

Figure 7: Circumferential variation of Axial Force, Radial Force and Torque around the impeller axis, for $S_r = 0.146$ corresponding to subsonic flow inside the impeller.

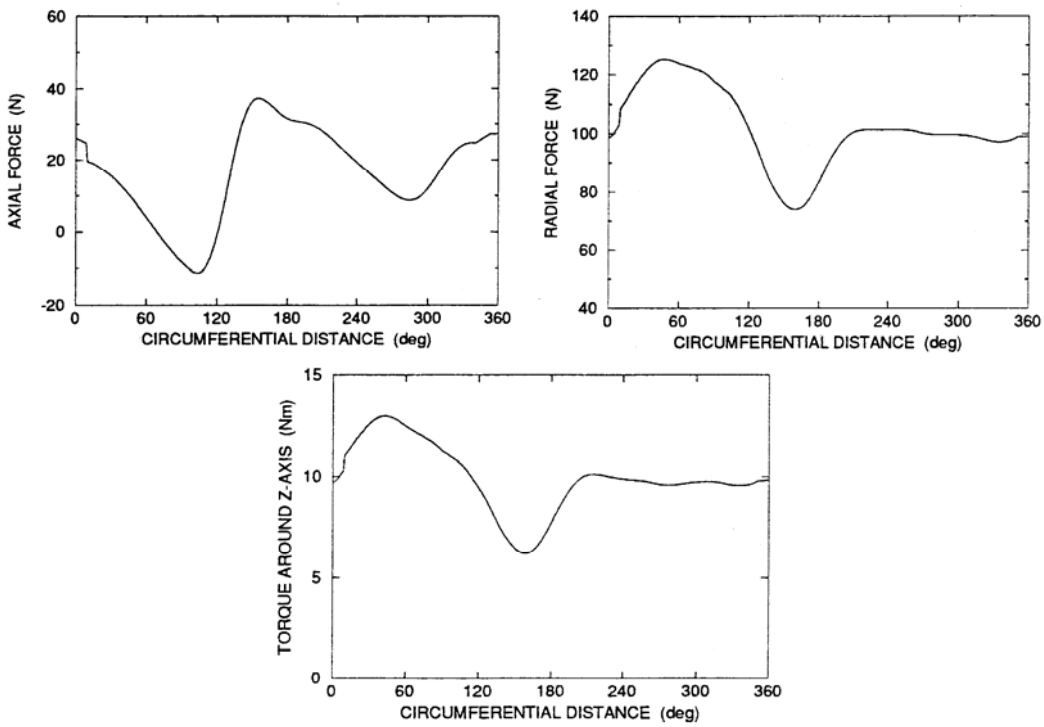

Figure 8: Circumferential variation of Axial Force, Radial Force and Torque around the impeller axis, for $S_s = 0.225$ corresponding to transonic flow inside the impeller.

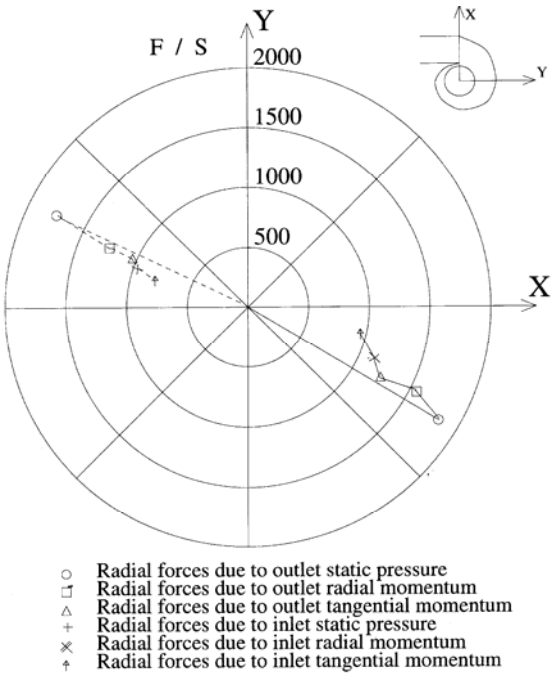

Figure 9: Components of radial force in the splitter-vaned impeller with backward leaned blades. Continuous lines correspond to higher mass flows, and dashed lines correspond to lower mass flows.

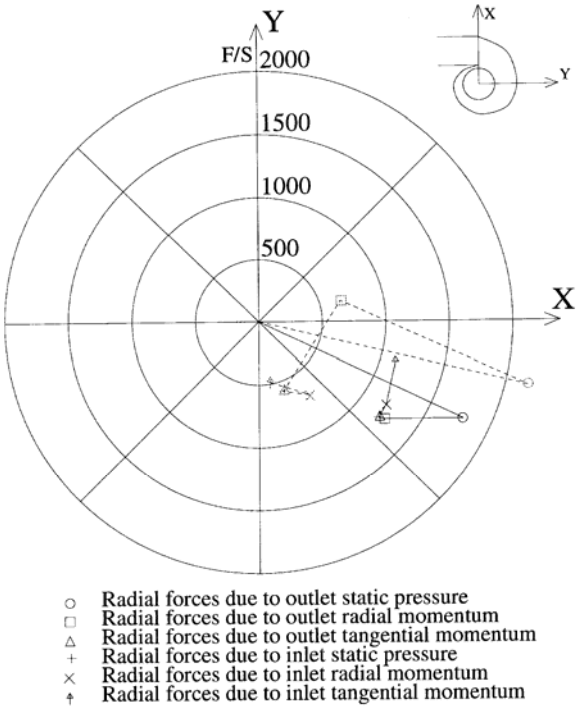

Figure 10: Components of Radial Force in an impeller with backward leaned (continuous lines), and radial ending blades (dashed lines)

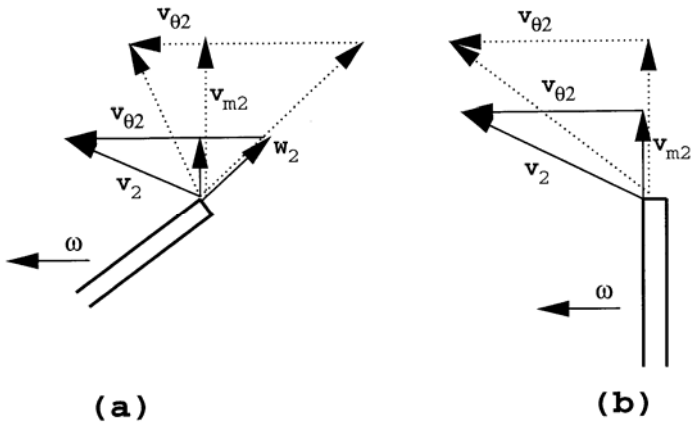

Figure 11: Difference in tangential momentum distribution between impeller with (a) backward leaned blades, and (b) radial ending blades

Experimental data mainly obtained in centrifugal pumps, confirm the existence of rotordynamic forces due to the static pressure fluctuations [18]. These forces are due to the response of the centrifugal impeller to the asymmetric static pressure imposed to the impeller outlet due to the volute [19]. Numerical results by means of commercial computer packages, confirm the prediction of the direction of the radial force acting on the bearings of the impeller shaft [20]. The unsteady forces on the impeller blades produce vibration and increase the noise of the compressor [21, 22].

Calculations were done for higher than optimum mass flows and for $S_r = 0.146$ corresponding to subsonic flow inside the impeller and for $S_r = 0.225$ corresponding to transonic flow conditions. For these cases it was found that the circumferential variations of the axial force, radial force and torque around the axis of the impeller are larger as the Strouhal number increases, which could lead to resonance conditions, as in the case of full-bladed centrifugal impeller, [1]. For the case of $S_r = 0.146$, a large variation of forces and torque is occurring at the circumferential position corresponding to the volute tongue. For the case of $S_r = 0.225$, a bimodal variation is observed for the forces and torque.

Calculations were also done for the case of higher and lower than the optimum mass flow. In the case of higher mass flows the unsteady flow phenomena are more pronounced than in the case of lower mass flow. The radial force direction for both cases is typical and is confirmed by many experimental observations, [16].

Two different methods were applied to compute the radial force caused by the static pressure distortion; namely the pressure integration and the momentum balance. From the calculations done it is shown that the momentum balance method is more sensitive to the grid density than the pressure integration method.

The different contributions to the radial forces are evaluated by means of the momentum balance method. The largest contribution is due to the variation of the outlet static pressure. The resulting radial force is larger at higher mass flows than at lower mass flows. This is also confirmed by experimental and numerical results in [23].

Integration of the static pressure at the impeller outlet section gives an approximation of the total radial force on the impeller with backward leaned blades. It is completely wrong for radial ending blades where the variation in radial momentum almost completely compensates the pressure forces. The difference in force direction is due to the large contribution of the tangential momentum force, perpendicular to the radial one.

The information provided by this study on the distribution of unsteady forces and torques acting on each individual blade can be used as input to calculate the mechanical structure of the impeller. It also helps to find the rotordynamic behaviour of the impeller shaft to the unsteady fatigue loading, [22].

References

[1] A. Fatsis, Computation of the 3-Dimensional Unsteady Flow in a Centrifugal Impeller due to a downstream Static Pressure Circumferential Distortion, 1995, Ph.D. Thesis, RUG-Von Karman Institute.

[2] R.J. Knapp, R.C. Binder, “Experimental Determinations of the Flow Characteristics in Volutes of Centrifugal Pumps”. Transactions of ASME, Vol. 58 1936, 649-663.

[3] H. Iversen, R. Rolling, J. Carlson, “Volute pressure distribution, Radial Force on the Impeller, and Volute Mixing Losses of a Radial Flow Centrifugal Pump”, ASME Journal Engineering for Power, Vol. 82, 1960, 136-144.

[4] Y. Hasegawa, K. Kikuyama, T. Maeda, Effects of blade number on Hydraulic Force perturbation on impeller of volute-type Centrifugal Pump. JSME International Journal, Series II. Vol. 33, 1990, 736-742.

[5] A.J. Stepanoff. Centrifugal and Axial Flow Pumps, second ed. New York: John Wiley and Sons, Inc;,1957.

[6] A. Agostinelli, D. Nobles, C.R. Mockridge, “An experimental investigation of radial thrust in centrifugal pumps”. ASME Journal of Engineering for Power. Vol. 82, 1960, 120-126.

[7] H.J. Biheller, "Radial force on the impeller of centrifugal pumps with volute, semivolute and fully concentric casings". ASME Journal Engineering for Power. Vol. 87, 1965, 319-323.

[8] G.T. Csanady, "Radial forces in a pump impeller caused by a volute casing". ASME Journal Engineering for Power, Vol. 84, 1962, 337-340.

[9] J.A. Lorett, S. Gopalakrishnan, S. "Interaction in between Impeller and Volute of Pumps at off-design conditions". ASME Journal Fluids Engineering, Vol.108, 1986.

[10] S.M. Miner, R.D. Flack, P. Trevisan, "Potential flow analysis of the forces on a laboratory centrifugal pump impeller". ASME Paper 92-GT-285.

[11] D. Croba. Modélisation de l'écoulement instationnaire dans les pompes centrifuges. Interaction roue-volute. 1992, PhD Thesis, Institut National Polytechnique de Grenoble.

[12] M. Sideris. Circumferential distortion of the flow in Centrifugal Compressors due to Outlet Volutes, 1988, Ph.D. Thesis, RUG-Von Karman Institute.

[13] A. Fatsis. Three dimensional unsteady flow calculations in radial components. 1993, Von Karman Institute Lecture Series 1993-01 'Spacecraft Propulsion'.

[14] J.I. Erdos, E. Alzner, "Computation of Unsteady Transonic Flows through rotating and stationary cascades", 1977, NASA CR 2900.

[15] D.W. Childs, "Pressure oscillation in the leakage annulus between a shrouded impeller and its housing due to impeller-discharge-pressure disturbances". ASME Journal of Fluids Engineering. Vol. 114, 1992, 61-67.

[16] J. Meier-Grotian. Untersuchungen der radialkraft auf das laufrad einer Kreiselpumpe bei verschiedenen Spiralgehaeuseformen, 1972, Ph.D. Thesis, T.U. Braunschweig.

[17] D. Hagelstein, K. Hillewaert, R. A. Van den Braembussche, A. Engeda, R. Keiper, M. Rautenberg, "Experimental and Numerical Investigation of the Flow in a Centrifugal Compressor Volute". ASME Journal of Turbomachinery, Vol. 122, No. 1, 2000, 22-32.

[18] M. Sinha, A. Pinarbasi, and J. Katz, "The Flow Structure During Onset and Developed States of Rotating Stall Within a Vaned Diffuser of a Centrifugal Pump". ASME Journal of Fluids Engineering, Vol.123, No. 3, 2001, 490-500.

[19] A. Hiwata, Y. Tsujimoto, "Theoretical Analysis of Fluid Forces on an Open-Type Centrifugal Impeller in Whirling Motion". ASME Journal of Fluids Engineering, Vol. 124, No. 2, 2002, 342-348.

[20] J.J. Moore, DL Ransom, F Viana, "Rotordynamic Force Prediction of Centrifugal Compressor Impellers Using Computational Fluid Dynamics". ASME Paper 2007-GT-28181.

[21] Q. Liu, D. Qi, Y. Mao, "Numerical calculation of centrifugal fan noise". Proceedings of the Institution of Mechanical Engineers, Part C: Journal of Mechanical Engineering Science, Vol. 220, No. 8, 2006, 1167-1177.

[22] H.-P. Dickmann, T. S. Wimmel, J. Szwedowicz, D. Filsinger, and Ch.H. Roduner "Unsteady Flow in a Turbocharger Centrifugal Compressor: Three-Dimensional Computational Fluid Dynamics Simulation and Numerical and Experimental Analysis of Impeller Blade Vibration", ASME Journal of Turbomachinery, Vol. 128, No. 3, 2006, 455-466

[23] M.Zhang, H. Tsukamoto, "Unsteady Hydrodynamic Forces due to Rotor-Stator Interaction on a Diffuser Pump With Identical Number of Vanes on the Impeller and Diffuser". ASME Journal of Fluids Engineering, Vol. 127, No. 4, 2005, 743-752.